Environmental Science & Technology

Article

Cite This: Environ. Sci. Technol. 2018, 52, 12783−12791

pubs.acs.org/est

# Self-Damaging Aerobic Reduction of Graphene Oxide by *Escherichia coli*: Role of GO-Mediated Extracellular Superoxide Formation

Huiru Zhao,[†] Chengdong Zhang,[*,‡] Yaqi Wang,[†] Wei Chen,[†] and Pedro J. J. Alvarez[§]

[†]College of Environmental Science and Engineering, Nankai University, Tianjin 300350, China

[‡]School of Environment, Beijing Normal University, Beijing 100857, China

[§]Department of Civil and Environmental Engineering, Rice University, Houston, Texas 77005, United States

Supporting Information

**ABSTRACT:** Microbial reduction of graphene oxide (GO) under aerobic conditions is poorly understood despite its critical role in changing GO toxicity and environmental fate. Here we show that 20 mg/L GO interacts with the membrane-bound cytochrome *c* of *E. coli* in saline, shuttling electrons from the respiratory chain to extracellular molecular oxygen. This results in the formation of superoxide anions ($O_2^{\bullet-}$), which in turn reduce GO in 30 min. The critical role of superoxide was demonstrated by impeding GO reduction upon addition of superoxide dismutase, or by carrying out experiments under strictly anaerobic conditions that preclude $O_2^{\bullet-}$ formation. Coating GO with bovine serum albumin also stopped GO reduction, which indicates the need for direct contact between GO and the cell membrane. Cell death was observed as a consequence of GO bioreduction. Apparently, electron shuttling by GO (via membrane contact) interrupts the respiratory chain and induces oxidative stress, as indicated by a 20% decrease in electron transport activity and an increase in intracellular reactive oxygen species. This novel antimicrobial mechanism could be relevant to assess GO stability and biocompatibility, and informs potential applications for microbial control.

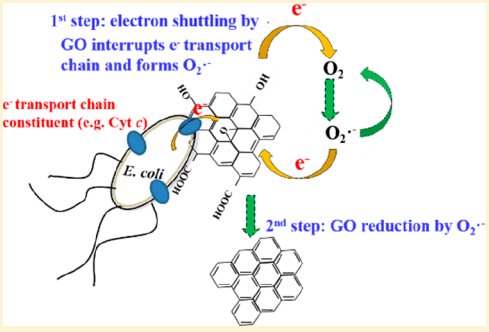




## INTRODUCTION

Owing to its electronic, mechanical, optical, and thermal properties, graphene oxide (GO) is being considered for many different applications.[1−5] Large-scale production of GO is conducive to incidental or accidental releases to the environment,[6] where it may undergo various transformations.[7−9] Among these transformations, GO reduction has received much attention because this process substantially alters GO toxicity.[10] For instance, reduced GO (rGO) is reported to be more toxic than the parent GO to both Gram-positive *Staphylococcus aureus* and Gram-negative *Escherichia coli*.[11] rGO exhibited stronger antimicrobial activity than GO against *E. coli*, with an inactivation efficiency of 84% versus 59%, respectively, after 1 h exposure.[11]

Microbial reduction of GO can be accomplished by various microorganisms under both anaerobic and aerobic conditions. GO can be reduced by heterotrophic, facultative anaerobes such as *Shewanella*,[12] *E. coli*,[13] and *Halomonas eurihalina*.[14] Two extracellular electron transfer pathways have been suggested: direct charge transfer from the cell surface and the use of self-secreted soluble redox electron mediators.[14,15] A few studies have shown that strictly anaerobic conditions are not required for microbial reduction of GO since this process can also occur aerobically.[16−18] Proposed explanations for aerobic GO reduction include that rapid utilization of oxygen by fast-growing cells results in an anaerobic microenvironment,[19] and that flexible GO sheets wrap themselves around the cell surfaces, locally decreasing oxygen availability.[12] However, rapid diffusion of oxygen under continuous stirring facilitates its presence during GO reduction, which requires an explanation of how GO competes successfully with oxygen as an electron acceptor. Furthermore, the role of oxygen in the GO reduction pathway and its interaction at GO-membrane interface are poorly understood.

Discerning the aerobic reduction mechanism is important to inform GO stability and fate and transport processes in the environment. Moreover, *E. coli* growth has been reported to be inhibited as a result of GO reduction.[10] Thus, uncovering the antimicrobial mechanism associated with aerobic reduction of GO is important to inform the durability and biocompatibility of graphene-based materials and to possibly enhance microbial control applications.

In this study we show that GO interacts with membrane-bound cytochrome *c* of *E. coli*, shuttling electrons from the respiratory chain to extracellular molecular oxygen. This results in the formation of superoxide anions ($O_2^{\bullet-}$), which in turn reduce GO. The reduction process interrupts the respiration chain and contributes significantly to the overall cytotoxicity.

Received: July 8, 2018
Revised: September 7, 2018
Accepted: October 2, 2018
Published: October 2, 2018




DOI: 10.1021/acs.est.8b03753
Environ. Sci. Technol. 2018, 52, 12783−12791

## MATERIALS AND METHODS

**Materials.** GO was purchased from Plannano, China. *E. coli* MP 1 was obtained from Agricultural Culture Collection of China (ACCC, Beijing). All reagents used in this study were of analytical grade or better.

**GO Bioreduction.** *E. coli* were grown in Luria−Bertani (LB) medium at 37 °C to midexponential phase and then harvested by centrifugation at 4500 rpm at 4 °C. After washing, cells were resuspended and diluted in saline (0.5% NaCl) to achieve the concentration of $10^7$−$10^8$ cfu/mL. GO was added to the cell suspension at a final concentration of 20 mg/L, and the mixture was incubated at 37 °C for 0.5 h with continuous shaking, which was sufficient to complete the bioreduction process until no further GO structural change was detected. To evaluate whether GO can be reduced by spent medium, GO was incubated in spent medium for 0.5 h instead of cell suspension. The spent medium was collected after microbial growth to midexponential phase via centrifugation. To validate the involvement of $O_2$, the bioreduction was also performed under anaerobic condition in an anaerobic chamber (1029 Forma Anaerobic System, Massachusetts, U.S.A.).

**GO and rGO Characterization.** After reduction, rGO were collected via centrifugation at 9000 rpm and purified according to Chouhan's method.[17] Briefly, the brownish pellet was phase separated in a mixture of 1:1 hexane/deionized water and centrifuged at 5000 rpm for 6 min. The rGO, which appeared at the interface of two solvent phases, was carefully collected, washed with deionized water, and dried in vacuum desiccator before characterization.

Surface elemental composition of the rGO were determined with X-ray photoelectron spectroscopy (XPS) (PHI 5000 VersaProbe, Tokyo, Japan). The crystal structures were determined with X-ray diffraction (XRD) using a D/Max-2500 diffractometer (Rigaku, Tokyo, Japan) working at 40 kV and 40 mA using CuK$\alpha$ radiation. Raman spectra were recorded using a Renishaw inVia Raman spectrometer (RM2000, London, U.K.) with an exciting wavelength of 532 nm. Fourier transform infrared (FTIR) transmission spectra of the materials were obtained using a 110 Bruker TENSOR 27 apparatus (Bruker Optics Inc., Karlsruhe, Germany). The particle size distribution of GO or rGO suspensions and $\zeta$ potential were measured by dynamic light scattering (DLS) using a ZetaPALS (Brookhaven Instruments, Holtsville, U.S.A.). Corresponding polydispersity index values with DLS measurements were provided in Table S1 of the Supporting Information (SI). And all measurements were done at least in triplicate, and the results were expressed as mean ± standard deviation (SD). Typically, the SD/mean for DLS measurement was in the range of 1.4%−9.5%. Sonication (at 40 kHz for 10 min) was used to ensure adequate dispersion before DLS and zeta potential measurements. The morphology was visualized via Scanning Electron Microscope (SEM, Nova Nano SEM 230, Hillsboro, U.S.A.).

**Interaction of Cyt *c* with GO.** According to Ma et al.,[20] 20 mg/L GO was added to 150 $\mu$g/mL Cyt *c* solution (from Macklin, China), and the spectral change were monitored by UV−vis spectrometer (Cary 100, California, U.S.A.) from 350 to 650 nm. Where it was needed, GO was preincubated with bovine serum albumin (BSA) before interaction with Cyt *c*. Briefly, 2.5 mL of 1 g/L GO was mixed with 1 mL of 10 g/L BSA and 1.5 mL of sterile water, and the mixture was incubated at 37 °C in an orbital shaker for 2 h. After that, BSA-coated GO was separated via centrifugation, and washed three times to remove unbounded protein. The size of conjugated particle and suspendability were also analyzed with DLS (Figure S1).

**$O_2^{\bullet-}$ Measurement.** *E. coli* was incubated with 20 mg/L of GO in saline for the indicated time, and the supernatant was separated by centrifugation at 4500 rpm for 9 min. Sodium-2,3,-bis(2-methoxy-4-nitro-5-sulfophenyl)-5-[(phenylamino)-carbonyl]-2H-tetrazolium inner salt (XTT, from Coolaber, China), a known superoxide trap, was added to the supernatant at a final concentration of 125 $\mu$M. The mixture was incubated at 37 °C for 2 h, and the absorption was measured at 450 nm by microplate reader (Synergy 4, Vermont, U.S.A.).[21] XTT in saline with 20 mg/L GO only was used as abiotic control. Some tests were conducted in the presence of dicumarol (0.2 mg/L), which inhibits Cyt *c* reductase[22] (a component of the respiratory chain), to evaluate how interruption of respiratory chain by GO contributes to toxicity. Specifically, dicumarol minimizes respiratory electron transport activity and associated shuttling to GO. Additional controls were used, including GO that had been preincubated (and coated) with 10 g/L BSA to determine the importance of direct cellular contact with GO, and with 0.2 mg/L of superoxide dismutase (SOD) to scavenge $O_2^{\bullet-}$ and discern its importance to GO reduction and cellular toxicity. In all cases, measurements uncertainties are calculated as the SD/mean, which was typically in the range of 2.3%−6.7%.

**Evaluation of Cell Viability and Oxidative Damage.** Bacteria were incubated with 20 mg/L of GO in saline for 2 h, in the presence or absence of SOD, dicumarol, or BSA. Cells were then collected, washed and subjected to 4′,6-diamidino-2-phenylindole/Propidium Iodide (DAPI/PI) staining (KeyGEN BioTECH, Nanjing, China).[23] Cell viability was also evaluated after incubation with GO under anaerobic conditions or with 20 mg/L of rGO. Images were acquired on a confocal microscope (LSM 880, Jena, Germany). The viability was also quantified with lactase dehydrogenase (LDH) release using a cytotoxicity detection kit (KeyGEN BioTECH, Nanjing, China).[24] During incubation, the intracellular reactive oxygen species (ROS) content was measured using a ROS detection kit (KeyGEN BioTECH, Nanjing, China).[24] The malondialdehyde (MDA) content and total glutathione/oxidized glutathione ratio (GSH/GSSH) over time were measured using a micro-MDA assay reagent kit (KeyGEN BioTECH, Nanjing, China) and assay kit (Nanjing Jiancheng Bioengineering Institute, China), respectively.

**Electron Transport Activity Assay.** The electron transport system activity of the *E. coli* was assessed by the reduction of 2-(*p*-iodophenyl)-3-(*p*-nitrophenyl)-5-phenyl tetrazolium chloride (INT) to formazan (INF).[25] The bacteria were harvested by centrifugation, washed twice with phosphate buffered saline (PBS, 50 mM, pH 7.4) buffer, and resuspended in 1 mL PBS. Then 200 $\mu$L of INT (0.5%) and 0.2 mg nicotinamide adenine dinucleotide (NADH) were added, the mixture was incubated at 30 °C for 30 min under dark. After the addition of 100 $\mu$L of formaldehyde to terminate the reaction, the cells were collected by centrifugation, and 500 $\mu$L of 96% methanol were used to extract INF from the cells. The extraction process was repeated twice, after which the extract was measured at 490 nm by microplate reader (Synergy 4, Vermont, U.S.A.) against a solvent blank. The electron transport activity was calculated as follows:[25]


DOI: 10.1021/acs.est.8b03753
Environ. Sci. Technol. 2018, 52, 12783−12791

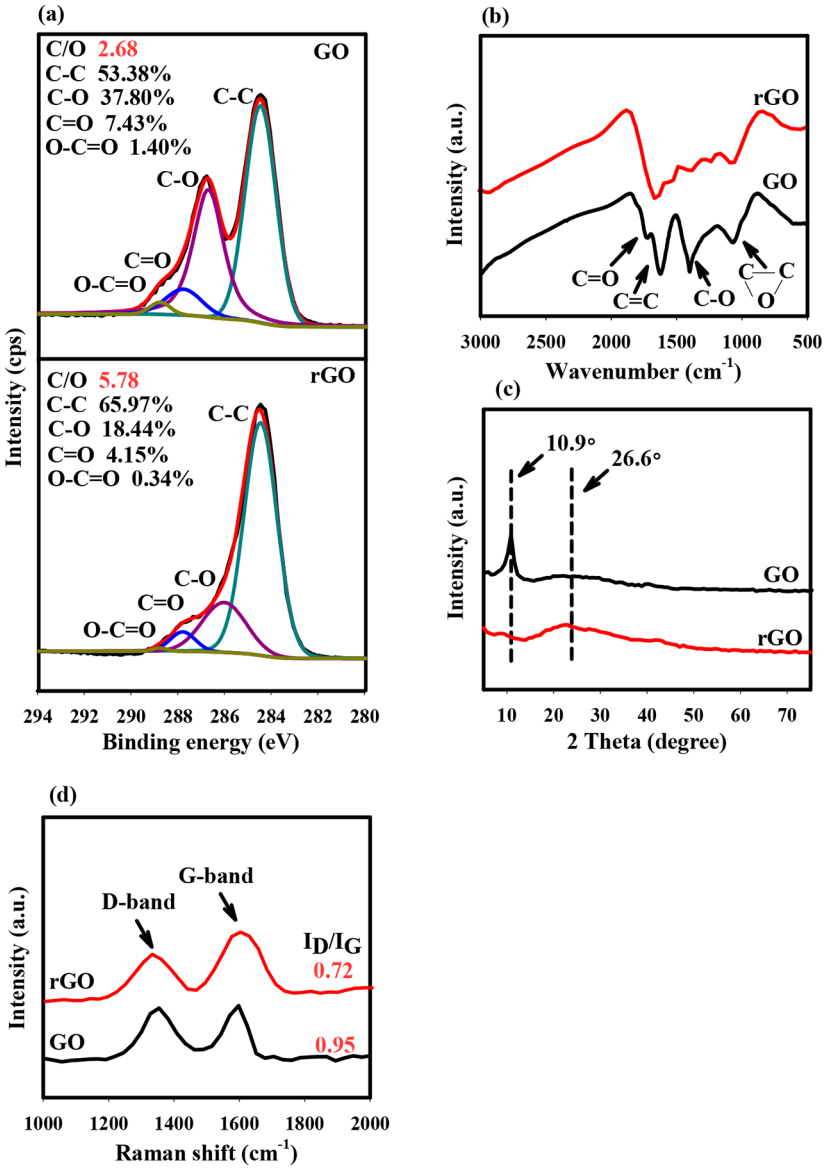


**Figure 1.** GO was bioreduced by *E. coli* under aerobic conditions. Reduced GO (rGO) was characterized by (a) XPS analysis; (b) FTIR spectroscopy; (c) XRD analysis; and (d) Raman spectroscopy. GO (20 mg/L) was incubated with *E. coli* for 2 h in saline solution.

$$\text{electron transport activity } (\mu gO_2 \cdot g^{-1}\text{protein} \cdot \text{min}^{-1}) = \frac{ABS_{490}}{15.9} \times \frac{V_1}{V_0 t} \times \frac{32}{2} \times \frac{1}{m}$$

where, $ABS_{490}$ is the sample absorbance, 15.9 is the specific absorptivity of INT−formazan, $V_0$ and $V_1$ are the initial volumes of bacteria and the total volume of methanol (mL), $t$ is the incubation time (min), 32/2 is the constant for transformation of $\mu$mol INT-formazan to $\mu$g $O_2$, and $m$ is the protein concentration (mg protein/mL bacteria). The precision of these measurements was reflected by the relatively low coefficient of variation of replicate analyses, which ranged from 3.0% to 4.8%.

**Statistical Analysis.** At least three replicates were run per treatment. For some experiment (i.e., bioreduction), experiments were repeated more than ten times. All data were expressed as means ± SD, and statistical difference was determined by independent $t$ test or One-Way ANOVA test. A $p$-value less than 0.05 (*) indicated significant difference.

## RESULTS AND DISCUSSION

**GO was Reduced by *E. coli* under Aerobic Conditions.** XPS, XRD, Raman, and FTIR spectroscopy results show that GO was considerably reduced after microbial incubation under aerobic conditions. The XPS spectrum of GO after incubation was similar to that reported for rGO,[26] and the C/O ratio increased to 5.78 in comparison with the value of 2.68 for pristine GO (Figure 1a). The decreases in the peak intensity of the epoxy/hydroxyl (at 286.30 eV), carbonyl (at 287.30 eV) and carboxyl groups (at 288.80 eV) were significant. Notably, the bacterial residues on the GO surface were completely removed (as indicated by the absence of a potassium ($2p_{3/2}$) peak at a binding energy of 292.7 eV) (Figure S2)[10] and did not interfere with the XPS analysis. The apparent reduction in O-containing groups on rGO, such as carbonyl (at 1735 $cm^{-1}$), alkoxyl (at 1055 $cm^{-1}$), and epoxy (at 1277 $cm^{-1}$),[26] was also substantiated by the FTIR spectra (Figure 1b).

GO bioreduction was further corroborated with XRD analysis (Figure 1c). The characteristic diffraction peak of pristine


DOI: 10.1021/acs.est.8b03753
Environ. Sci. Technol. 2018, 52, 12783−12791

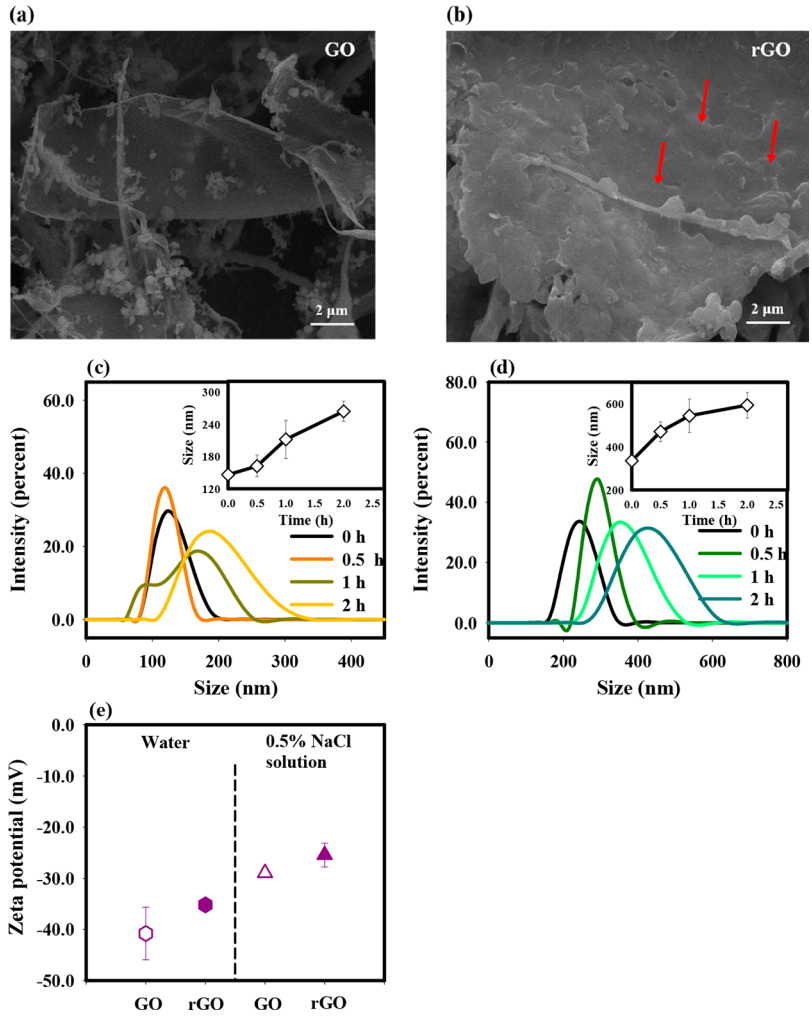


**Figure 2.** Distinct morphological and physical properties of rGO compared to GO. SEM images of (a) GO and (b) rGO. Red arrows point to appearance of holes and wrinkles on the rGO surface. Size distribution of (c) GO and (d) rGO indicates that the latter formed larger aggregates. The inserts depict an increase in hydrodynamic diameters over time. (e) Zeta potentials of rGO and GO both in water and in saline solution. All experiments were carried out at least in triplicate.

GO appeared at 10.9°, whereas after reduction, the peak intensity became indiscernible, and the appearance of wide peak at 26.6° indicated the formation of rGO.[27] The change of XRD pattern was likely due to the alteration of interlayer spacing and ordering of the 2D structure. Consistent with this result, the intensity ratio of the D and G bands ($I_D/I_G$) of GO in the Raman spectrum was approximately 0.95, while the $I_D/I_G$ of rGO was 0.72 due to the removal of oxygen-containing functional groups (Figure 1d). The decrease in the $I_D/I_G$ ratio indicated the reduction in structural defects as a result of $sp^2$ network recovery. This trend for the $I_D/I_G$ ratio was consistent with that reported for bacterially reduced GO.[17]

Bioreduction is also evident by the change in the morphological properties, surface charge and aggregation behavior of GO after microbial incubation (Figure 2). The morphology change can be visualized in SEM images that after reduction thick and bulky aggregates were observed in comparison with transparent and thin-layered pristine GO (Figure 2a and b). The hydrodynamic diameter of rGO was generally more than twice larger than that of GO, suggesting that rGO tended to aggregate due to the increased hydrophobicity from reduction (Figure 2c and d). Also, rGO was less negatively charged relative to pristine GO both in water and in saline because of the loss of O-containing functional groups (Figure 2e). Collectively, the changes of physical and morphological properties corroborate that GO had been microbially transformed to its reduced form.

**Extracellular $O_2^{\bullet-}$ was Responsible for GO Reduction.** Since it has been suggested that GO might be reduced by bacterial-secreted extracellular substances or under created anaerobic microenvironments,[10,28,29] we excluded these possibilities by incubating GO with spent medium or by performing the incubation under strictly anaerobic conditions. As shown in Figure 3a, no GO reduction was observed under either condition (as indicated by the similar $I_D/I_G$ ratios). Other mechanisms may be responsible for microbial reduction of GO, in which both oxygen and direct contact with cell (possibly involving aerobic respiratory activity) are required.

Since many bacterial cells are able to produce extracellular $O_2^{\bullet-}$,[30,31] and $O_2^{\bullet-}$ can act as both reductant and oxidant, we first explored whether biogenerated extracellular $O_2^{\bullet-}$ may have contributed to GO reduction. As shown in Figure 3b, we detected nearly 3-fold formation of $O_2^{\bullet-}$ during the first 30 min of incubation, which coincided with GO reduction. Furthermore, no GO reduction was detected after the addition


DOI: 10.1021/acs.est.8b03753
Environ. Sci. Technol. 2018, 52, 12783−12791

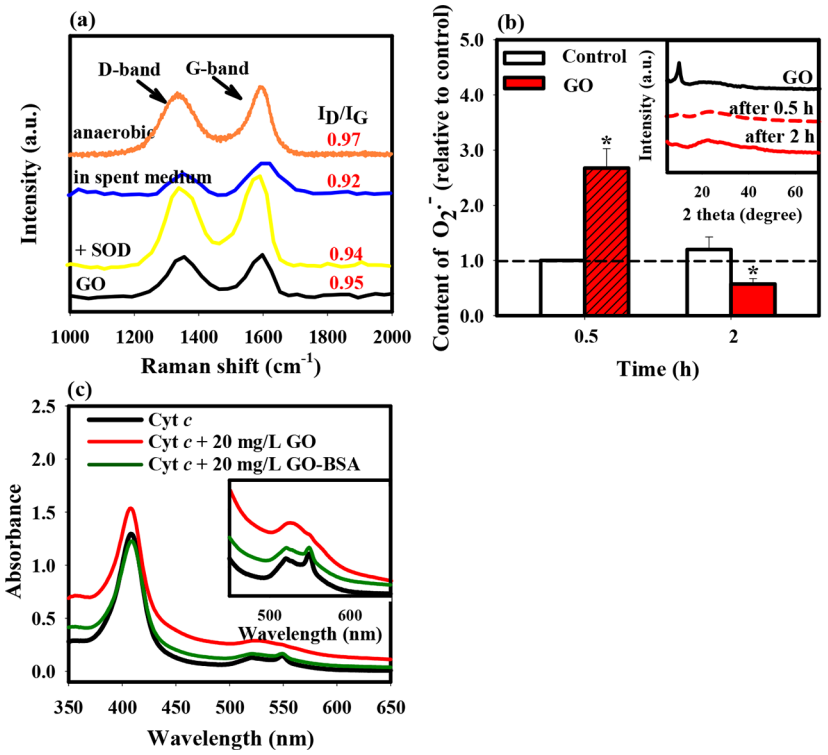


**Figure 3.** GO was bioreduced by extracellular $O_2^{\bullet-}$. (a) Raman spectra of GO under various incubation conditions. (b) Production of extracellular $O_2^{\bullet-}$ over time. The insert shows XRD spectra of GO at different incubation times. (c) UV−vis spectra of Cyt *c* during interaction with GO or BSA-coated GO. The insert enlarges the spectra in the range of 450−650 nm. *E. coli* was incubated with GO (20 mg/L) for 2 h unless otherwise indicated. Cyt *c* (150 μg/mL) was incubated with 20 mg/L GO. Some treatments were amended with 0.2 mg/L SOD or 10 g/L of BSA. These experiments were carried out at least in triplicate, and results were given as the mean values ± standard deviations. The asterisks (*) indicate a significant difference ($P < 0.05$) relative to controls.

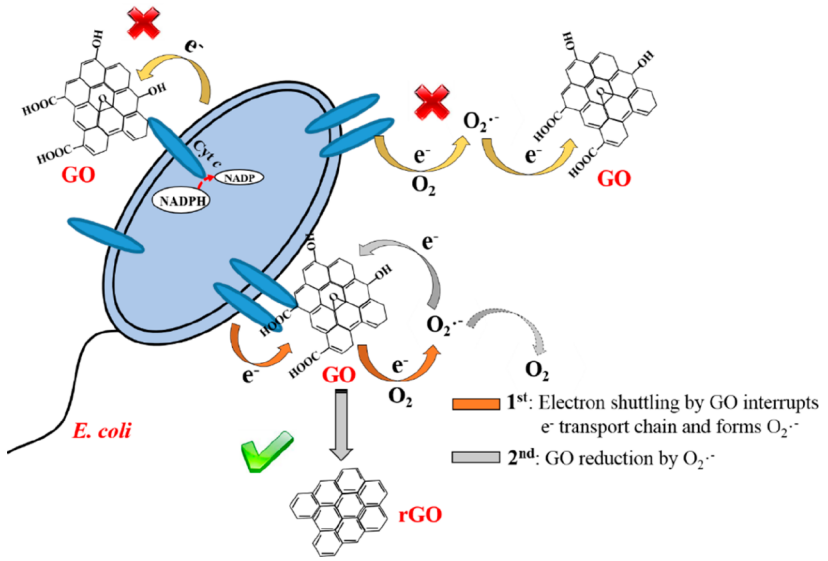


**Figure 4.** Bioreduction mechanism.

of SOD, a $O_2^{\bullet-}$ scavenger, which indicates that $O_2^{\bullet-}$ plays a critical role in GO reduction (Figure 3a). The reduction of GO by $O_2^{\bullet-}$ was verified using an abiotic $O_2^{\bullet-}$ generation system (Figure S3).

**$O_2^{\bullet-}$ was Formed via Electron Shuttling by GO.** Some membrane-bound electron transport chain constituents, such as Cyt *c*, relay electrons from the respiration chain toward the outer part of the membrane,[32] resulting in reduction of $O_2$ to $O_2^{\bullet-}$.[32] We hypothesized that GO may interact with Cyt *c* or other respiratory chain constituents, facilitating the electron transfer process and promoting $O_2^{\bullet-}$ production. We therefore investigated the interaction between Cyt *c* (which is a cross-membrane protein) and GO. As shown in Figure 3c, the reduced form of Cyt *c* showed peaks at 520 and 550 nm, and after interaction with 20 mg/L GO, the protein exhibited a wide peak at approximately 530 nm (red line), which was


DOI: 10.1021/acs.est.8b03753
Environ. Sci. Technol. 2018, 52, 12783−12791

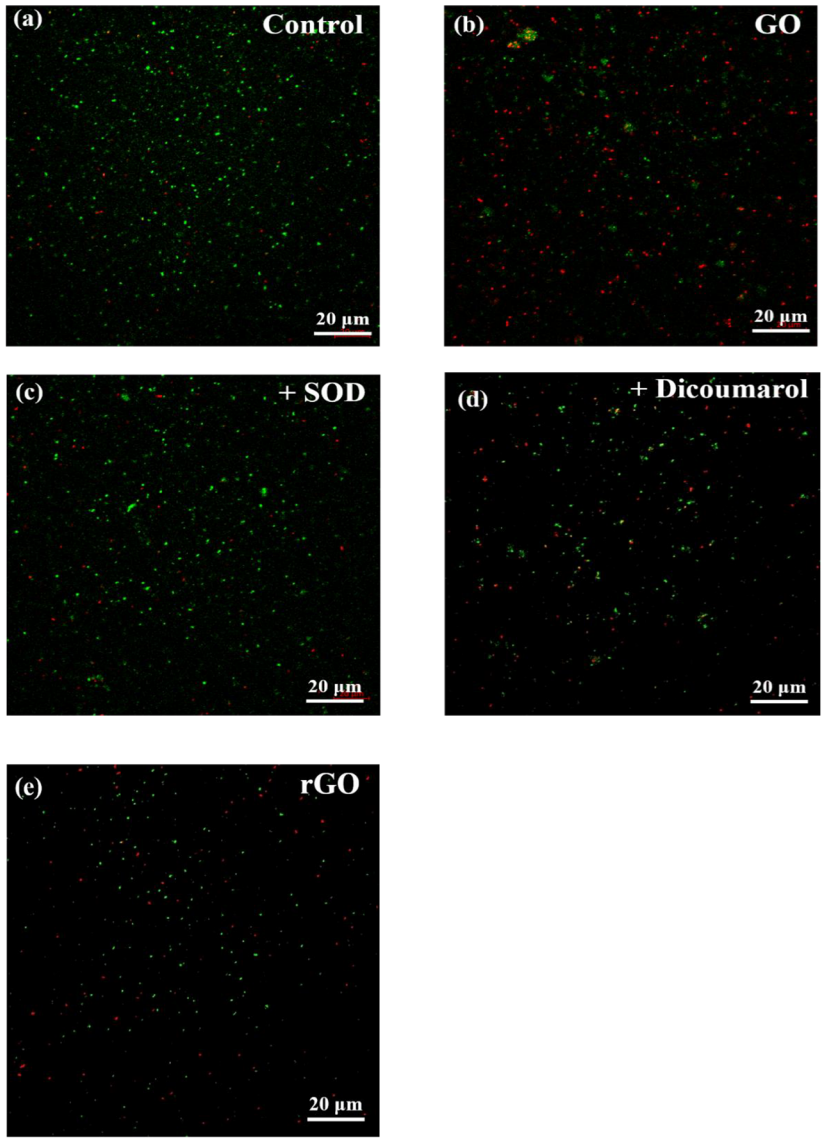


**Figure 5.** Confocal microscopy images showing that the GO reduction contributed significantly to microbial toxicity. The cell viabilities of (a) control, or in the presence of (b) GO; (c) GO + SOD; (d) GO + dicoumarol; and (e) rGO as indicated by DAPI/PI stain. Dead cells were stained in red by PI while live cells were stained in green by DAPI. The concentration of GO or rGO was 20 mg/L in all experiments. Some treatments were amended with 0.2 mg/L SOD or 0.2 mg/L dicoumarol. These experiments were carried out at least in triplicate.

indicative of an oxidized form of Cyt *c*.[33] However, when GO was coated with BSA, no spectral change was observed, supporting the hypothesis that Cyt *c* can directly transfer electrons to GO and itself becomes oxidized. These electrons were further shuttled by GO to extracellular $O_2$, expediting $O_2^{\bullet-}$ production (Figure 3b). Electron-shuttling by GO has been previously reported.[14,28] GO is known to shuttle electrons from NADH to molecular oxygen, promoting $O_2^{\bullet-}$ production.[34] Here, we demonstrate a novel (aerobic) GO bioreduction pathway where GO accepts electrons from cross-membrane protein Cyt *c* (and possibly other components of the electron transfer chain) and shuttles them to extracellular $O_2$ to form $O_2^{\bullet-}$, which in turn reduces GO (Figure 4).

Direct contact of GO with the cell membrane was a prerequisite for the observed $O_2^{\bullet-}$ generation activity since neither $O_2^{\bullet-}$ overproduction nor GO reduction was observed when GO was precoated with BSA (Figure S4). Protein corona formation was indicated by the significant increase in GO particle size (Figure S1).

**This GO Reduction Process Contributed Significantly to Cellular Death.** The proposed GO reduction mechanism (Figure 4) would be harmful to the cell by interrupting the respiratory chain and inducing $O_2^{\bullet-}$-related oxidative stress. Accordingly, whereas significant cell death was observed concurrently with GO reduction (Figure 5a and b), no GO reduction was detected (Figure S4) and cell viability was preserved (Figure 5c and d) in the presence of SOD (to remove $O_2^{\bullet-}$) or dicumarol (a Cyt *c* reductase inhibitor[22] to minimize electron transport activity and associated shuttling to GO). We further quantified loss of cell viability by measuring LDH release, and bioreduction-induced release was almost five times of that observed for unexposed *E. coli* (Figure 6a). Bacterial inactivation was also noted in a dose-dependent manner (with GO concentrations ranging from 5 to 20 mg/L) concomitant with GO reduction (Figure S5). Consistently, cell death significantly decreased when no GO reduction (and associated escape of electrons from the respiratory chain) occurred (Figure 6).


DOI: 10.1021/acs.est.8b03753
*Environ. Sci. Technol.* 2018, 52, 12783−12791

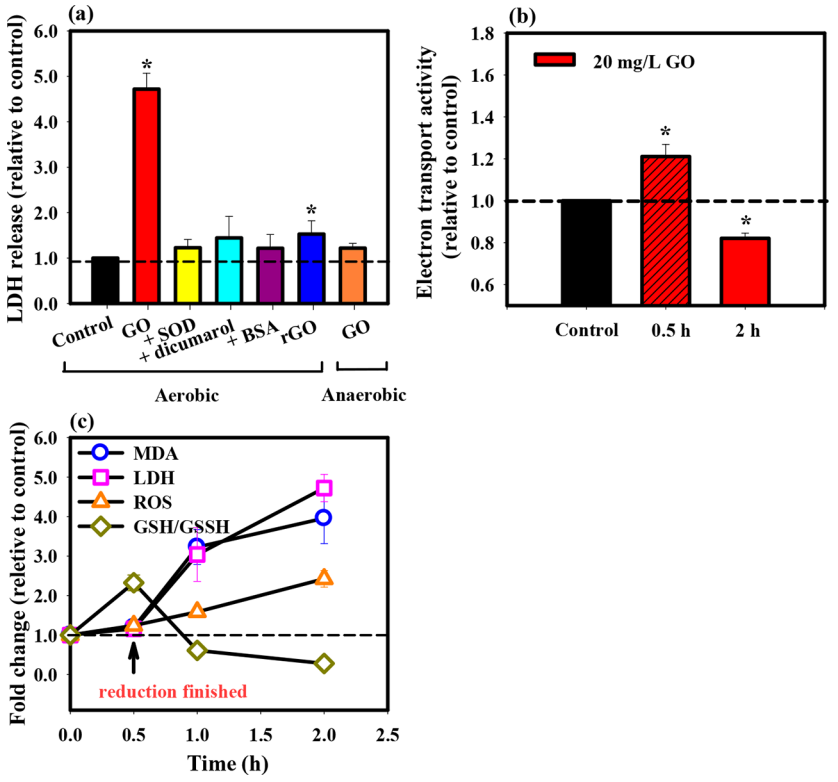


**Figure 6.** Microbial toxicity was only related to GO reduction. (a) LDH release under various incubation conditions. (b) The change of electron transport system activity during incubation. (c) Changes of MDA, LDH, ROS content, and GSH/GSSH ratio over time. In all experiments, *E. coli* was incubated with 20 mg/L GO (or rGO) for 2 h in saline solution. Experiments were carried out at least in triplicate and results were given as the mean values ± standard deviations. The asterisks (*) indicate a significant difference ($P < 0.05$) relative to controls.

The antimicrobial effect of GO had been previously ascribed to two major mechanisms: physical disruption of the membrane (i.e., penetration, extraction) and chemical oxidation either through direct contact with the membrane or via intrinsic ROS generation.[35,36] Both mechanisms can be excluded here by experiments where cell viability was preserved upon direct contact of GO with the cell membrane under conditions that mitigated GO reduction and oxidative stress (e.g., with dicumarol or SOD, or under anaerobic conditions) (Figure 6a). Note that hydrogen peroxide ($H_2O_2$) that could have been produced by superoxide reduction was not a significant contributor to toxicity or GO reduction under the tested conditions. Specifically, biogenerated superoxide is converted to $H_2O_2$ by SOD,[37] and no GO reduction (Figure 3a) or toxicity (Figure 6a) was observed in SOD-amended incubations. Direct toxicity of rGO can also be ruled out since no appreciable toxic effect was observed when rGO was incubated with *E. coli* under the same conditions (Figure 5e). Although rGO is generally more conductive than GO,[38] it formed larger aggregates in saline and precipitated quickly, thus minimizing cellular contact (Figure 2c).

To verify that cytotoxicity was largely due to the interruption of respiratory chain via electron transfer to GO, we monitored the change in electron transport activity during incubation (Figure 6b). Exposure to GO increased electron transport activity by more than 20% during the first 30 min of incubation. A significant decrease in electron transport activity was eventually observed after 2 h, which was attributed to oxidative stress as indicated by the decrease in GSH/GSSH ratio (Figure 6c).

GO has been previously proposed to exert oxidative stress by oxidizing GSH,[39] thereby depleting the bacterial antioxidant system. To elucidate the direct contribution of GSH oxidation to GO reduction and cytotoxicity, we monitored the GSH/GSSF ratio as well as several indicators of oxidative stress during GO bioreduction (Figure 6c). Although GO was reduced in 30 min (Figure 3b), GSH depletion was notably delayed. This suggests that the electrons for GO reduction were transferred mainly from the respiratory chain rather than directly from GSH oxidation. Furthermore, intracellular ROS content, lipid peroxidation (MDA content), and LDH release started to increase after 30 min, peaking after 2 h. Therefore, GSH depletion was mainly a consequence of oxidative stress, rather than direct GO reduction.

Overall, GO served as a conductive bridge to shuttle electron from the intracellular respiratory chain to extracellular molecular oxygen, thereby promoting $O_2^{\bullet-}$ production, which in turn reduced GO and the reduction process caused severe oxidative damage. This novel (aerobic) bioreduction mechanism could be important to inform the fate and transport of GO in the environment, assess GO stability and biocompatibility, and design GO-based materials with tunable conductivity for some microbial control applications.

## ■ ASSOCIATED CONTENT

### Supporting Information

The Supporting Information is available free of charge on the ACS Publications website at DOI: 10.1021/acs.est.8b03753.

DLS and polydispersity index (PDI) of different concentration of GO in solutions over time; the size distribution change of BSA-coated GO over time in saline; the overall spectra of XPS analysis for pristine GO and bioreduced GO; the Raman spectra shows that GO was



DOI: 10.1021/acs.est.8b03753
Environ. Sci. Technol. 2018, 52, 12783−12791

reduced by abiotically generated $O_2^{\bullet-}$; the content of $O_2^{\bullet-}$ under various incubation conditions and corresponding Raman spectra of GO after incubation; and the cell viability (as measured by LDH release) drops in a dose-dependent manner concomitant with reduction (PDF)

## AUTHOR INFORMATION


### Corresponding Author

*Phone/fax: 86-10-58802029; e-mail: zhangchengdong@bnu.edu.cn.

### ORCID

Chengdong Zhang: 0000-0002-1100-2584
Wei Chen: 0000-0003-2106-4284
Pedro J. J. Alvarez: 0000-0002-6725-7199


### Notes

The authors declare no competing financial interest.

## ACKNOWLEDGMENTS

This project was supported by the National Natural Science Foundation of China (Grants 21777077 and 81373039) and the Ministry of Science and Technology of China (Grant 2014CB932001), and the Fundamental Research Funds for the Central Universities (310432102). Partial support was also provided by the NSF ERC on Nanotechnology-Enabled Water Treatment (EEC-1449500).

## REFERENCES


(1) Karim, M. R.; Hatakeyama, K.; Matsui, T.; Takehira, H.; Taniguchi, T.; Koinuma, M.; Matsumoto, Y.; Akutagawa, T.; Nakamura, T.; Noro, S. Graphene oxide nanosheet with high proton conductivity. *J. Am. Chem. Soc.* **2013**, *135* (22), 8097−8100.

(2) Wei, J.; Hu, Y. X.; Liang, Y.; Kong, B. A.; Zhang, J.; Song, J. C.; Bao, Q. L.; Simon, G. P.; Jiang, S. P.; Wang, H. T. Nitrogen-doped nanoporous carbon/graphene nano-sandwiches: synthesis and application for efficient oxygen reduction. *Adv. Funct. Mater.* **2015**, *25* (36), 5768−5777.

(3) Li, X. L.; Wang, X. R.; Zhang, L.; Lee, S. W.; Dai, H. J. Chemically derived, ultrasmooth graphene nanoribbon semiconductors. *Science* **2008**, *319* (5867), 1229−1232.

(4) Mohanty, N.; Berry, V. Graphene-based single-bacterium resolution biodevice and DNA transistor: interfacing graphene derivatives with nanoscale and microscale biocomponents. *Nano Lett.* **2008**, *8* (12), 4469−4476.

(5) Kauffman, D. R.; Star, A. Graphene versus carbon nanotubes for chemical sensor and fuel cell applications. *Analyst* **2010**, *135* (11), 2790−2797.

(6) Du, T. T.; Adeleye, A. S.; Keller, A. A.; Wu, Z. N.; Han, W.; Wang, Y. Y.; Zhang, C. D.; Li, Y. Photochlorination-induced transformation of graphene oxide: mechanism and environmental fate. *Water Res.* **2017**, *124*, 372−380.

(7) Zhang, C. D.; Chen, S. L.; Alvarez, P. J. J.; Chen, W. Reduced graphene oxide enhances horseradish peroxidase stability by serving as radical scavenger and redox mediator. *Carbon* **2015**, *94* (11), 531−538.

(8) Zhao, J.; Wang, Z. Y.; White, J. C.; Xing, B. S. Graphene in the aquatic environment: adsorption, dispersion, toxicity and transformation. *Environ. Sci. Technol.* **2014**, *48* (17), 9995−10009.

(9) Fu, H. Y.; Qu, X. L.; Chen, W.; Zhu, D. Q. Transformation and destabilization of graphene oxide in reducing aqueous solutions containing sulfide. *Environ. Toxicol. Chem.* **2014**, *33* (12), 2647−2653.

(10) Akhavan, O.; Ghaderi, E. *Escherichia coli*. bacteria reduce graphene oxide to bactericidal graphene in a self-limiting manner. *Carbon* **2012**, *50* (5), 1853−1860.

(11) Akhavan, O.; Ghaderi, E. Toxicity of graphene and graphene oxide nanowalls against bacteria. *ACS Nano* **2010**, *4* (10), 5731−5736.

(12) Wang, G. M.; Qian, F.; Saltikov, C. W.; Jiao, Y. Q.; Li, Y. Microbial reduction of graphene oxide by *shewanella*. *Nano Res.* **2011**, *4* (6), 563−570.

(13) Raveendran, S.; Chauhan, N.; Nakajima, Y.; Toshiaki, H.; Kurosu, S.; Tanizawa, Y.; Tero, R.; Yoshida, Y.; Hanajiri, T.; Maekawa, T. Ecofriendly route for the synthesis of highly conductive graphene using extremophiles for green electronics and bioscience. *Part Part Syst. Char.* **2013**, *30* (7), 573−578.

(14) Bansal, P.; Doshi, S.; Panwar, A. S.; Bahadur, D. Exoelectrogens leading to precise reduction of graphene oxide by flexibly switching their environment during respiration. *ACS Appl. Mater. Interfaces* **2015**, *7* (37), 20576−20584.

(15) Shi, L.; Dong, H. L.; Reguera, G.; Beyenal, H.; Lu, A. H.; Liu, J.; Yu, H. Q.; Fredrickson, J. K. Extracellular electron transfer mechanisms between microorganisms and minerals. *Nat. Rev. Microbiol.* **2016**, *14* (10), 651−662.

(16) Gurunathan, S.; Han, J. W.; Eppakayala, V.; Kim, J. H. Microbial reduction of graphene oxide by escherichia coli: a green chemistry approach. *Colloids Surf., B* **2013**, *102* (2), 772−777.

(17) Chouhan, R. S.; Pandey, A.; Qureshi, A.; Ozguz, V.; Niazi, J. H. Nanomaterial resistant microorganism mediated reduction of graphene oxide. *Colloids Surf., B* **2016**, *146*, 39−46.

(18) Gurunathan, S.; Han, J. W.; Eppakayala, V.; Kim, J. H. Biocompatibility of microbially reduced graphene oxide in primary mouse embryonic fibroblast cells. *Colloids Surf., B* **2013**, *105* (6), 58−66.

(19) Reiling, H. E.; Laurila, H.; Fiechter, A. Mass culture of escherichia coli: medium development for low and high density cultivation of escherichia coli B/r in minimal and complex media. *J. Biotechnol.* **1985**, *2* (3), 191−206.

(20) Ma, X. W.; Zhang, L. H.; Wang, L. R.; Xue, X.; Sun, J. H.; Wu, Y.; Zou, G. Z.; Wu, X.; Wang, P. C.; Wamer, W. G. Single-walled carbon nanotubes alter cytochrome c electron transfer and modulate mitochondrial function. *ACS Nano* **2012**, *6* (12), 10486−10496.

(21) Gurunathan, S.; Han, J. W.; Dayem, A. A.; Eppakayala, V.; Park, M. R.; Kwon, D. N.; Kim, J. H. Antibacterial activity of dithiothreitol reduced graphene oxide. *J. Ind. Eng. Chem.* **2013**, *19* (4), 1280−1288.

(22) Liu, Y. N.; Zhang, F.; Li, J.; Li, D. B.; Liu, D. F.; Li, W. W.; Yu, H. Q. Exclusive extracellular bioreduction of methyl orange by azo reductase-free geobacter sulfurreducens. *Environ. Sci. Technol.* **2017**, *51* (15), 8616−8623.

(23) Liu, J. L.; Rojas-Andrade, M. D.; Chata, G.; Peng, Y.; Roseman, G.; Lu, J. E.; Millhauser, G. L.; Saltikov, C.; Chen, S. W. Photo-enhanced antibacterial activity of ZnO/graphene quantum dot nanocomposites. *Nanoscale* **2018**, *10* (1), 158−166.

(24) Zhang, Y. B.; Ali, S. F.; Dervishi, E.; Xu, Y.; Li, Z. R.; Casciano, D.; Biris, A. S. Cytotoxicity effects of graphene and single-wall carbon nanotubes in neural phaeochromocytoma-derived PC12 cells. *ACS Nano* **2010**, *4* (6), 3181−3186.

(25) Wan, R.; Chen, Y. G.; Zheng, X.; Su, Y. L.; Li, M. Effect of $CO_2$ on microbial denitrification via inhibiting electron transport and consumption. *Environ. Sci. Technol.* **2016**, *50* (18), 9915−9922.

(26) Wang, F. F.; Wang, F.; Gao, G. D.; Chen, W. Transformation of graphene oxide by ferrous iron: environmental implications. *Environ. Toxicol. Chem.* **2015**, *34* (9), 1975−1982.

(27) Zhou, X. J.; Zhang, J. L.; Wu, H. X.; Yang, H. J.; Zhang, J. Y.; Guo, S. W. Reducing graphene oxide via hydroxylamine: a simple and efficient route to graphene. *J. Phys. Chem. C* **2011**, *115* (24), 11957−11961.

(28) Salas, E. C.; Sun, Z. Z.; Lüttge, A.; Tour, J. M. Reduction of graphene oxide via bacterial respiration. *ACS Nano* **2010**, *4* (8), 4852−4858.

(29) Jiao, Y.; Qian, F.; Li, Y.; Wang, G. M.; Saltikov, C.; Gralnick, J. Deciphering the electron transport pathway for graphene oxide reduction by Shewanella oneidensis MR-1. *J. Bacterial.* **2011**, *193* (14), 3662−3665.




DOI: 10.1021/acs.est.8b03753
*Environ. Sci. Technol.* 2018, 52, 12783−12791

(30) Zhang, T.; Hansel, C. M.; Voelker, B. M.; Lamborg, C. H. Extensive dark biological production of reactive oxygen species in brackish and freshwater ponds. *Environ. Sci. Technol.* **2016**, *50* (6), 2983−2993.
(31) Diaz, J. M.; Hansel, C. M.; Voelker, B. M.; Mendes, C. M.; Andeer, P. F.; Zhang, T. Widespread production of extracellular superoxide by heterotrophic bacteria. *Science* **2013**, *340* (6137), 1223−1226.
(32) Campian, J. L.; Gao, X. S.; Qian, M. W.; Eaton, J. W. Cytochrome *c* oxidase activity and oxygen tolerance. *J. Biol. Chem.* **2007**, *282* (17), 12430−12438.
(33) Nakashima, T.; Sano, M. Single-walled carbon nanotube as 1D array of reacting sites: reaction kinetics of reduction of cytochrome c in tris buffer. *J. Phys. Chem. C* **2011**, *115* (43), 20931−20936.
(34) Zhao, Y. C.; Hsieh, H. S.; Wang, M.; Jafvert, C. T. Light-independent redox reactions of graphene oxide in water: electron transfer from NADH through graphene oxide to molecular oxygen, producing reactive oxygen species. *Carbon* **2017**, *123*, 216−222.
(35) Zheng, H. Z.; Ma, R. L.; Gao, M.; Tian, X.; Li, Y. Q.; Zeng, L. W.; Li, R. B. Antibacterial applications of graphene oxides: structure-activity relationships, molecular initiating events and biosafety. *Sci. Bull.* **2018**, *63* (2), 133−142.
(36) Ji, H. W.; Sun, H. J.; Qu, X. G. Antibacterial applications of graphene-based nanomaterials: recent achievements and challenges. *Adv. Drug Delivery Rev.* **2016**, *105*, 176−189.
(37) Korshunov, S.; Imlay, J. A. Detection and quantification of superoxide formed within the periplasm of escherichia coli. *J. Bioact.* **2006**, *188* (17), 6326−6334.
(38) Liu, S. B.; Zeng, T. H.; Hofmann, M.; Burcombe, E.; Wei, J.; Jiang, R.; Kong, J.; Chen, Y. Antibacterial activity of graphite, graphite oxide, graphene oxide, and reduced graphene oxide: membrane and oxidative stress. *ACS Nano* **2011**, *5* (9), 6971−6980.
(39) Chong, Y.; Ge, C. C.; Fang, G.; Wu, R. F.; Zhang, H.; Chai, Z. F.; Chen, C. Y.; Yin, J. J. Light-enhanced antibacterial activity of graphene oxide, mainly via accelerated electron transfer. *Environ. Sci. Technol.* **2017**, *51* (17), 10154−10161.


DOI: 10.1021/acs.est.8b03753
*Environ. Sci. Technol.* 2018, 52, 12783−12791